Background-free fluorescence decay time sensing and imaging of pH with highly photostable diazaoxotriangulenium dyes

Irene Dalfen,[1] Ruslan I. Dmitriev,[2,3] Gerhard Holst,[4] Ingo Klimant,[1] Sergey M. Borisov[1*]

1. Institute of Analytical Chemistry and Food Chemistry, Graz University of Technology, Stremayrgasse 9, 8010 Graz, Austria

2. School of Biochemistry and Cell Biology, University College Cork, Cork, Ireland

3. Institute for Regenerative Medicine, I.M. Sechenov First Moscow State University, Moscow, Russian Federation

4. PCO AG, Donaupark 11, 93309 Kelheim, Germany

* sergey.borisov@tugraz.at

ABSTRACT

Novel fluorescent diazaoxatriangulenium (DAOTA) pH indicators for lifetime-based self-referenced pH sensing are reported. The DAOTA dyes were decorated with phenolic receptor groups inducing fluorescence quenching via photoinduced electron transfer mechanism. Electron-withdrawing chlorine substituents ensure response in the most relevant pH range (apparent pK'_a values ~5 and 7.5 for the *p,p*-dichlorophenol- and the *p*-chlorophenol-substituted dyes, respectively). The dyes feature long fluorescence lifetime (17-20 ns), high quantum yield (~60%) and high photostability. Planar optodes are prepared upon immobilization of the dyes into polyurethane hydrogel D4. Apart from the response in the fluorescence intensity, the optodes show pH-dependent lifetime behaviour which makes them suitable for studying 2D pH distribution with help of fluorescence lifetime imaging technique. The lifetime response is particularly pronounced for the sensors with high dye concentration (0.5-1% wt. in respect to the polymer) and is attributed to efficient homo-FRET mechanism.

KEYWORDS

Decay time; FRET; pH sensor; triangulenium; photoinduced electron transfer, Frequency Domain FLIM

INTRODUCTION

Many biological and ecological systems are based on a delicate equilibrium between a wide range of different parameters. One of the most important is the pH, which is of highest importance in biology, biotechnology, medicine, oceanography and environmental monitoring to mention only a few fields. For monitoring pH in these areas, fluorescent chemosensors proved to be promising analytical tools since they are free from electromagnetic interferences, enable non-invasive measurements and are available in a variety of formats ranging from planar optodes and fiber optic sensors to nanoparticles.[1] In contrast to other methods (e.g. electrochemical sensing) optical sensors enable imaging of pH

distribution on surfaces (with help of planar optodes) or in volume (with help of nanoparticles). Particularly, planar optodes have been applied for imaging of pH gradients in marine sediments,[2,3] rhizosphere,[4,5] biofilms,[6] wounds[7,8] and microfluidic chips.[9,10]

Optical pH sensors are generally manufactured via immobilization of a pH indicator into a proton-permeable matrix, which ensures reusability of the sensor for multiple measurements. Among numerous fluorescent pH probes reported[11] some most common representatives are xanthene dyes,[12,13] derivatives of 8-hydroxypyrene-1,3,6-trisulfonic acid (HPTS),[14,15] naphthalimides[16,17] and BODIPY dyes.[18–20] Unfortunately, the performance of pH sensors based on UV-Vis indicators can be compromised by high levels of background fluorescence originating from biological species present in the analysed sample or from optical components such as fibers and filters. An additional optical isolation layer helps to minimize the autofluorescence in case of fiber-optic sensors and planar optodes but it can also introduce problems associated with interaction of the dye and the components of optical isolation (e.g. carbon black), and it is of course not possible at all in case of nanosensors. NIR excitable/emissive probes such as seminaphthorhodafluors (SNARFs)[21], aza-BODIPYs[22] and dyes of other classes proved to be advantageous due to low autofluorescence background in the NIR region. Unfortunately, most of these dyes have significantly lower fluorescence quantum yields compared to UV-Vis dyes.

Another way to overcome the above limitation is to use an indicator with comparably long luminescence decay time τ. Here, the background fluorescence can be eliminated in a time-resolved measurement. Luminescent pH probes based on metal complexes (most prominently Ru(II)[23–25] and Eu(III)[26] complexes) proved to be particularly interesting candidates due to their decay times in microsecond time domain. Apart from background-free measurements, some of these probes enable self-referenced decay time read-out[23,24] which is highly interesting for practical applications. Much more common intensity-based indicators require addition of a luminescent reference to the sensor material to ensure reliable read-out.[1–10] This in turn may introduce numerous issues associated with chemical and photochemical stability of the reference luminophore, leaching, oxygen cross-talk, inhomogeneous distribution of the two components, inner-filter effects etc. In respect to the pH indicators based on phosphorescence, long decay time typically results in a significant cross-sensitivity to molecular oxygen which has to be compensated for. Although several fluorescent indicators with decay time read-out have been reported, they either show comparably short wavelength of excitation and emission[27] or feature fairly short decay times (< 7 ns in the “on” state),[21,28,29] which makes background-free measurements problematic. Some nanosensors based on quantum dots feature significantly longer decay time and represent promising materials for pH sensing[30–32] but toxicity and environmental impacts may be a limitation here.

Therefore, fluorescent dyes with decay times long enough to eliminate the autofluorescence[33] but short enough to avoid cross-sensitivity to oxygen, are of high interest as an alternative platform for designing advanced pH optodes. Rich and co-workers showed that 90% of the background

fluorescence in tissues originates from emitters with the decay time of < 2.5 ns and about 10% from emitters with $\tau \sim 7.5$ ns.[33] Therefore, the overall autofluorescence is expected to decrease by about 10-fold after 7.5 ns which appears to be a reasonable threshold for designing lifetime-based sensors for *in vivo* applications. Among very few known representatives of the dyes with long fluorescence decay time,[34] triangulenium dyes[33,35] are particularly interesting due to combination of $\tau \sim 20$ ns and comparably long wavelengths of absorption and emission which are similar to those of the established chromophores such as rhodamines and BODIPYs. Although the pH-sensitive trihydroxytrioxatriangulene has been reported,[36] the fluorescence lifetimes of this dye do not exceed 4.3 ns in any protonation/deprotonation state, thus eliminating the strongest advantage of this dye group. While this work was in progress, Sørensen and co-workers reported a pH sensor based on a diazaoxatriangulenium ($DAOTA^+$) dye decorated with a phenolic receptor.[37] Since the sensing material has been characterized only for the fluorescence intensity, it remained unclear if the lifetime properties of the chromophore were affected by modification and immobilization.

In this contribution, the modification of diazaoxatriangulenium dyes with phenolate-based pH receptors was chosen as a pathway to obtain pH indicators with long-lived fluorescence and attractive spectral properties. These groups modulate the fluorescence of the dye via photoinduced electron transfer (PET) but do not affect the advanced photophysical properties of the chromophore. Incorporated in hydrogel matrices and nanoparticles the new indicators possess self-reference character due to lifetime sensing capabilities, which favourably distinguishes them from most systems presented so far. As will be demonstrated, planar optodes are particularly attractive for recording of pH distribution with fluorescence lifetime imaging (FLIM) technique.

EXPERIMENTAL

Materials

Chemicals were purchased from various commercial providers (TCI (www.tcichemicals.com), Fluka (www.analytics-shop.com/de/hersteller/fluka.html), Sigma Aldrich (www.sigmaaldrich.com), Acros Organics (www.acros.com), Roth (www.carlroth.com/at/de), ABCR (www.abcr.de)) and used as received. Macrolex Fluorescent Red G (3-(1,3-benzothiazol-2-yl)-7-(diethylamino)-2-oxo-2H-chromene-4-carbonitrile) from TER chemicals (www.terchemicals.com) and the perylene dye Lumogen Red from Kremer Pigmente (www.kremer-pigmente.com/de). Solvents were acquired from VWR (https://at.vwr.com/store) and used without further purification.

Eudragit RL-100 copolymer (poly-(ethylacrylate-co-methylmethacrylate-co-trimethyl-aminoethyl methacrylate), (average MW ≈ 150000 Da, 8.85 – 11.96 wt. % trimethyl-aminoethyl methacrylate units on dry substance) was from Degussa (www.evonik.com). Polyurethane hydrogels (Hydromed™ D1 and D4) were purchased from CardioTech (www.cardiotech-inc.com). Poly(methyl methacrylate-co-methacrylic acid (PMMA-MA, MW ≈ 100000 Da, 10% methacrylic acid) and poly(hydroxyethylmethacrylate) (pHEMA) (MW ≈ 150000 Da) were obtained from Polysciences Inc.

(www.polysciences.com). Poly(styrenesulfonic acid), (PSSA, MW ≈ 300000 Da), was from ABCR (www.abcr.de) and Nafion® 117 (5% wt. solution in alcohols) from Aldrich. Poly(ethylene terephthalate) support Melinex 505 was purchased from Pütz (www.puetz-folien.com).

Synthesis

Synthesis of fluorescent DAOTA dyes was conducted similar to procedures reported previously by Laursen et al.[38–40] Synthesis of tris(2,6-dimethoxyphenol)methanol (**a**) was performed according to the literature procedures.[41,42]

Synthesis of N-(3,5-dichloro-4-hydroxy)phenyl-N-dodecyl DAOTA$^+$ PF_6^- ***(PhOHCl$_2$-DAOTA)***

1.25 g (2.84 mmol) of **a** were dissolved in ethanol and acidified with 1 mL aqueous HBF_4 (50 wt%, 16.1 mmol). After precipitation with cyclohexane and filtration the solid was dissolved in acetonitrile. 508 mg (2.86 mmol) of 3,5-dichloro-4-hydroxyaniline and a few drops of pyridine were added under stirring at room temperature. The resulting orange intermediate was precipitated in 250 mL 0.2 M aqueous KPF_6 and collected via filtration. The precipitate was dissolved in N-methylpyrrolidone and 2.73 g (14.7 mmol) dodecylamine were added. After 1 h of stirring at 95 °C under argon atmosphere, the intermediate was precipitated with aqueous KPF_6 solution and isolated via filtration. It was dissolved in molten PyHCl and the melt stirred at 180 °C for 45 min. **PhOHCl$_2$-DAOTA** was isolated via precipitation from aqueous KPF_6 and filtration. The product was purified via flash column chromatography on silica with DCM/MeOH (99/1 v/v). Yield: 97 mg (5%).

^{1}H NMR (300 MHz, CD_3OD): δ = 8.08 (td, J =8.4, 5.5 Hz, 2 H, aromat. CH), 7.91 – 7.79 (m, 1 H, aromat. CH), 7.59 (d, J =8.9 Hz, 1 H, aromat. CH), 7.46 (d, J =8.6 Hz, 1 H, aromat. CH), 7.27 (d, J =8.2 Hz, 1 H, aromat. CH), 7.20 (d, J =13.6 Hz, 3 H, 1 H: triangulenium aromat. CH, 2 H: substituent aromat. CH), 6.84 (d, J =8.6 Hz, 2 H, aromat. CH), 4.58 – 4.41 (m, 2 H, N-CH_2), 1.92 (p, J =8.1, 7.6 Hz, 2 H, aliphat. CH_2), 1.62 (p, J =7.2 Hz, 2 H, aliphat. CH_2), 1.46 (dq, J =11.6, 6.1, 5.3 Hz, 2 H, aliphat. CH_2), 1.31 (d, J =16.4 Hz, 16 H, aliphat. CH_2), 0.95 – 0.81 (m, 3 H, CH_3).

^{13}C APT-NMR (76 MHz, CD_3OD): δ = 145.10, 143.64, 142.04, 140.82, 140.18, 139.53, 128.27, 127.89, 112.17, 110.63, 109.95, 109.05, 107.30, 64.72, 49.00, 33.34, 31.03, 30.72, 27.91, 27.20, 24.00, 14.71

MS MALDI-TOF: *m/z* [M^+] calc. 611.22, found 611.12.

Synthesis of N-(3-chloro-4-hydroxy)phenyl-N-dodecyl DAOTA$^+$ PF_6^- ***(PhOHCl-DAOTA)***

The dye was prepared analogously to **PhOHCl$_2$-DAOTA** using 3-chloro-4-hydroxyaniline instead of 3,5-dichloro-4-hydroxyaniline. Yield: 32 mg (4%).

^{1}H NMR (300 MHz, CD_2Cl_2): δ = 8.13 (t, J =8.5 Hz, 1H, aromat. CH), 8.04 (t, J =8.6 Hz, 1 H, aromat. CH), 7.97 – 7.81 (m, 2H, 1 H: triangulenium aromat. CH, 1 H: substituent *p*-OH aromat. CH), 7.48 (d, J =8.8 Hz, 1 H, aromat. CH), 7.43 – 7.27 (m, 4 H, 3 H: Triangulenium aromat. CH, 1 H: substituent *p*-

Cl aromat. CH), 7.19 – 7.07 (m, 1 H, substituent aromat.CH), 6.87 – 6.73 (m, 2 H, aromat. CH), 4.51 (t, *J* =8.3 Hz, 2 H, N-CH_2), 2.00 (p, *J* =7.5 Hz, 2 H, aliphat. CH_2), 1.71 – 1.54 (m, 2 H, aliphat. CH_2), 1.45 (s, 2 H, aliphat. CH_2), 1.40 – 1.11 (m, 14 H, aliphat. CH_2), 0.88 (t, *J* =6.5 Hz, 3 H, CH_3).

^{13}C APT-NMR (76 MHz, CD_2Cl_2): δ =145.10, 143.64, 142.04, 140.82, 140.18, 139.53, 128.27, 127.89, 112.17, 110.63, 109.95, 109.05, 107.30, 64.72, 49.00, 33.34, 31.03, 30.72, 27.91, 27.20, 24.00, 14.71

MS MALDI-TOF: *m/z* [M^+] calc. 577.26, found 577.25.

Synthesis of N-(3-Morpholinopropyl)-N-dodecyl DAOTA$^+$ PF_6^- ***(Morph-DAOTA)***

Synthesis of Morph-DAOTA was conducted similarly to that of **PhOHCl$_2$-DAOTA** and **PhOHCl-DAOTA**. The order of substitution was reversed with the dodecyl chain introduced before the morpholino group. Yield: 34 mg, 10%.

^{1}H NMR (300 MHz, CD_2Cl_2): δ = 8.28 (t, 1H, aromat. C-H), 8.09 (t, 2H, aromat. C-H), 7.84 (d, J =4.7 Hz, 1H, aromat. C-H), 7.78 – 7.67 (m, 1H, aromat. C-H), 7.49 (d, J =8.3 Hz, 1H, aromat. C-H), 7.40 (d, J =7.6 Hz, 1H, aromat. C-H), 7.27 (d, J =4.3 Hz, 2H, aromat. C-H), 4.73 (s, 2H, N-CH2), 4.59 – 4.39 (m, 2H, N-CH2), 3.77 (s, 3H, morpholino N-CH_2), 3.70 – 3.48 (m, 3H, propyl N-CH_2), 2.65 (d, J =35.1 Hz, 4H, morpholino N-CH_2), 2.13 (d, J =10.5 Hz, 2H, propyl CH_2), 1.93 (s, 2H, aliphat. CH_2), 1.61 (s, 2H, aliphat. CH_2), 1.42 (s, 3H, aliphat. CH_2), 1.26 (s, 10H, aliphat. CH_2), 0.86 (d, J =6.7 Hz, 3H, CH_3)

^{13}C APT-NMR (76 MHz, CD_2Cl_2): δ = 153.16, 141.63, 141.30, 140.54, 140.39, 140.14, 139.28, 112.01, 110.23, 109.59, 109.29, 107.99, 107.02, 106.35, 100.54, 67.25, 54.00, 48.94, 46.93, 32.45, 30.10, 29.87, 27.30, 26.26, 23.22, 14.42, 8.53

MS MALDI-TOF: *m/z* [M^+] calc. 578.37, found 578.25.

Optode Preparation

A solution containing 10% wt. polymer (Hydromed D4 polyurethane hydrogel) and 0.1% wt. dye (1 wt. % in respect to polymer) in EtOH:H_2O (9:1 v/v) was knife coated onto a poly(ethylene terephthalate) support with a bar film applicator (75 µm wet film thickness) and the solvent was allowed to evaporate under ambient conditions. For the optodes containing 0.5, 0.3 and 0.15 % wt. of PhOHCl$_2$-DAOTA in hydrogel D4 the thickness of the wet film was 75, 200 and 200 µm, respectively. This way, inner filter effect was avoided at higher dye concentrations and sufficient brightness of the optodes was ensured at lower dye concentrations. For imaging experiments diamond micropowder (1:1 w/w in respect to the polymer) was added to the sensor foil (1% dye w/w with respect to polymer).

Preparation of Nanoparticles and *investigation of their properties in solutions and in cells* is reported in supporting information.

Measurements

^{1}H and ^{13}C NMR spectra were recorded on a Bruker AVANCE III instrument (300.36 MHz ^{1}H NMR, 75.53 MHz ^{13}C NMR). Mass spectra were acquired in a positive reflector mode on a Micromass TofSpec 2E Time-of-Flight Mass Spectrometer (Bruker Ultraflex Extreme, www.bruker.com).

Absorption spectra were measured on a Varian Cary 50 UV-VIS spectrometer (www.agilent.com) in 10 mm precision cuvettes by Hellma Analytics (www.hellma-analytics.com). Emission spectra were recorded on a Hitachi-F-7000 fluorescence spectrometer (www.hitachi-hightech.com). Fluorescence lifetimes were acquired using time correlated single photon counting technique (TCSPC) on a FluoroLog® 3 spectrofluorometer (Horiba Scientific, www.horiba.com). Excitation was performed with a NanoLED (λ = 453 nm) controlled by a Delta Hub module and a pulse length of 1.1 ns. The average decay times were obtained from the fit of the decay profiles with biexponential decay model. Absolute quantum yields were determined on the FluoroLog® 3 spectrofluorometer equipped with a Quanta-Φ integrating sphere. Relative quantum yields were determined against Lumogen Red as reference dye (Φ = 0.96[43]).

Nanoparticle size and surface charge were determined on a particle size analyzer Zetasizer Nano ZS (www.malvernpanalytical.com).

Photostability measurement

Photostability of PhOHCl-DAOTA was investigated in comparison with Macrolex® Fluorescent Red G and Rhodamine 101. The absorption of solutions of PhOHCl-DAOTA and the reference dyes in EtOH was measured every five minutes while illuminating the solutions with a high power LED (λ = 528 nm) (www.led-tech.de). The photon flux of the LED was measured using a LI-250A Light Meter from LI-COR Biosciences (www.licor.com) and was 11700 µmol s^{-1} m^{-2}, 9100 µmol s^{-1} m^{-2} and 8400 µmol s^{-1} m^{-2} for PhOHCl-DAOTA, Macrolex® Red and Rhodamine 101, respectively. The decrease in absorption was corrected to normalize the values for the identical light intensity.

pH Calibrations

Unless otherwise stated, all measurements were conducted at 25 °C with buffer concentration of 10 mM and ionic strength adjusted with NaCl. Absorption and emission spectra for the optode based on $PhOHCl_2$-DAOTA in D4 (1% wt.) were acquired at pH values between 3 and 9 in buffers with 10 mM buffer concentration and additional salt concentrations of 10 mM NaCl, 290 mM NaCl, 290 mM $NaNO_3$ and 100 mM $NaClO_4$ plus 190 mM NaCl. Boltzmann sigmoid function was used to fit the response curves: $y = A_2 + \frac{A_1 - A_2}{1 + e^{\frac{pH - pKa'}{dx}}}$, where A_2 and A_1 are the lower and upper limits of the calibration function, respectively, pK_a' is the point of inflection of the sigmoid and *dx* describes the slope in the point of inflection.

FD-FLIM Imaging

Imaging experiments were performed with a pco.flim camera from PCO (www.pco.de/de) operating in the frequency domain.[44,45] The excitation source, a 488 nm laser diode (PhoxXplus 488-200 for pco.flim) from Omicron (www.omicron-laser.de), was modulated at 15 MHz modulation frequency (square wave modulation). Average laser power was 100 mW. The NIS Elements AR microscopy software from Nikon was used for data acquisition and processing. For microscopic measurements the sensor spots of 5 mm in diameter were cut out of the sensor foil and glued into a black 96 microwell plate from Greiner bio-one (www.gbo.com). Images were acquired with a Nikon Eclipse Ti-S microscope equipped with a Nikon Plan Apo 20x/0.75 objective and 0.7x camera adaptor mounted on the camera. The filter cube included an excitation bandpass filter FF02-482/18, a dichroic mirror Di02-R488 and an emission longpass filter BLP01-488R, all from Semrock (www.semrock.com). A dye-doped plate UMM/SFG from Starna Scientific (www.starna.com) was used as a lifetime standard (τ = 3.75 ns).

For macroscopic measurements, the sensor foil was fixed in the channel of the open microfluidic chip (COP polymer, ChipShop, www.microfluidic-chipshop.com) with an epoxy glue. The chip was bonded using a double side adhesive tape from ChipShop. The laser light was coupled into a 3 mm liquid waveguide in combination with beam expansion optics to homogenously illuminate the microfluidic chamber under observation. A longpass filter OG 530 from Schott (www.schott.de) was used in front of the macro lens Zeiss Makro-Planar 2/100 mm ZF (www.zeiss.com). Polystyrene-immobilized Lumogen red was used as a lifetime standard (τ = 6.3 ns as determined in TCSPC experiments).

RESULTS AND DISCUSSION

Synthesis

Although triangulenium dyes have been primarily chosen for their extraordinary long fluorescence lifetimes (~20 ns), these dyes also feature comparably long wavelengths of absorption and emission (particularly for di-aza substituted representatives), which is favourable for biological applications. The triangulenium structure offers a straightforward synthetic strategy to introduce functional groups (Scheme 1). The dyes were substituted with a dodecyl chain on one nitrogen bridge as a hydrophobic anchor to achieve good solubility in organic solvents and to prevent leaching from polymer matrices. A pH-sensitive functionality was introduced via the second nitrogen bridge. Two different moieties were investigated. The first group includes phenolic receptors which are known to induce efficient quenching via photoinduced electron transfer when deprotonated.[46] Importantly, the pK_a of the receptor can be tuned via the number of electron-withdrawing chlorine atoms attached to the phenyl ring. Mono- and dichloro-substituted phenols (PhOHCl-DAOTA and $PhOHCl_2$-DAOTA, respectively) were selected to cover the most relevant applications. A tertiary amine (morpholino group, Morph-

DAOTA) was chosen as the second receptor group. This group is potentially useful to achieve incomplete PET-quenching rendering both forms of the indicator emissive.

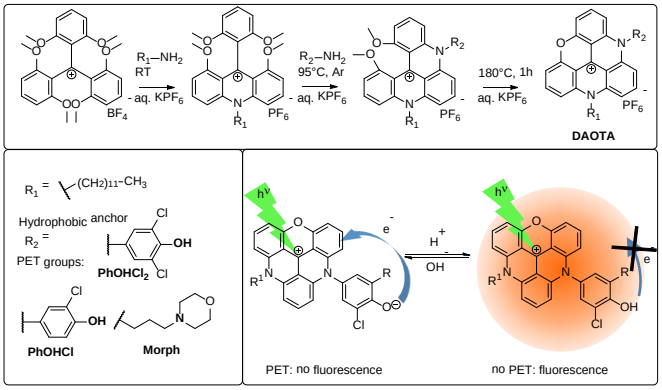

Scheme 1: Synthesis of new pH sensitive DAOTA dyes and sensing mechanism of the indicators.

Photophysical properties

Absorption and emission spectra are similar for the new DAOTA dyes substituted with different PET groups. The absorption and the emission maxima are located at ~560 and 590, respectively, resulting in a 30 nm Stokes shift (Figure **1**, Table **1**). The fluorescence quantum yields are comparable to those determined by Laursen et al. for the dipropyl-DAOTA dye (58% in acetonitrile)[47] with values between 48 and 63% in EtOH acidified with ~0.1% trifluoroacetic acid (TFA). Good quantum yields compensate for moderate molar absorption coefficients of $10 - 14 \cdot 10^3$ L mol^{-1} cm^{-1} ensuring acceptable brightness of the dyes. The fluorescence lifetimes are in the range of 17 to 19 ns in EtOH solution (Table **1**), as has been expected for DAOTA compounds. The fluorescence of PhOHCl-DAOTA and $PhOHCl_2$-DAOTA is strongly quenched upon deprotonation of the receptor (Figure **1**). In contrast, we did not observe any pH sensitivity for the Morph-DAOTA indicating that the tertiary amine is not an efficient PET quencher for the triangulenium chromophore.

Since luminescence of some cationic dyes is known to be efficiently quenched by chloride ions[48,49], this potential cross-talk was investigated. As can be seen from Figure S-20 (ESI), chloride ions do not notably affect the fluorescence properties of the triangulenium dyes even at very high concentration of 290 mM.

Table 1: Photophysical properties of DAOTA$^+$ dyes in ethanol, acidified with ~0.1% TFA.

	$\lambda_{max, abs}$ **[nm]**	$\lambda_{max, em}$ **[nm]**	**ε [L mol^{-1} cm^{-1}]** (n=3)	**Φ$^{(a)}$ [%]** (n=6)	**τ [ns]** (n=3)
$PhOHCl_2$-DAOTA	562	589	13800 ± 1400	63 ± 18	17.3 ± 0.1
PhOHCl-DAOTA	562	590	10600 ± 700	59 ± 7	17.7 ± 0.1
Morph-DAOTA	559	589	9800 ± 100	48 ± 12	19.0 ± 0.9

(a) Fluorescence quantum yields are determined as an average value of the absolute and relative quantum yields

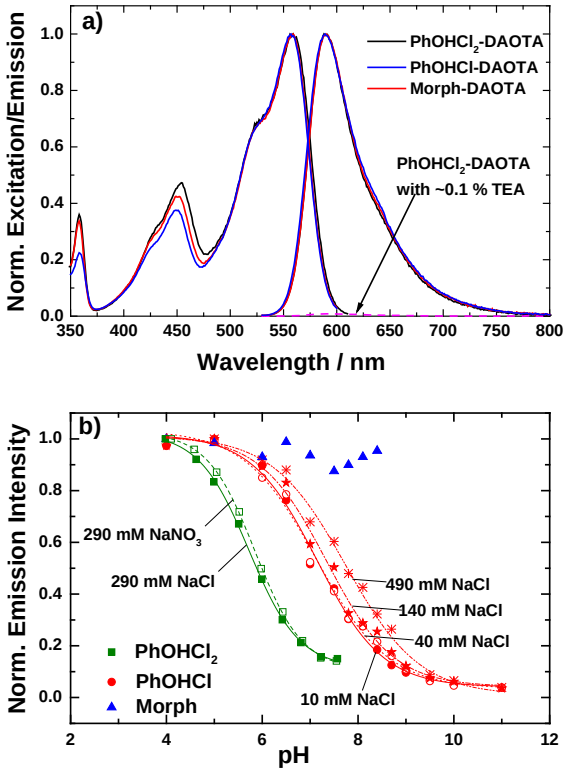

Figure 1: a) Absorption and emission spectra for the dyes in EtOH solution (except otherwise stated, all the solutions were acidified with ~0.1% TFA) **b)** calibration plots for the dyes dissolved in EtOH : aqueous buffer (1:1 v/v). The buffer concentration in the solution was 10 mM, the salt (NaCl or $NaNO_3$) concentration is indicated for each calibration; (λ_{exc} = 560 nm, λ_{em} = 590 nm).

Photostability

To access the photostability of the triangulenium system, the EtOH solution of PhOHCl-DAOTA was illuminated with a high power green LED. Two fluorescent dyes with similar spectral properties were used for comparison: the coumarin dye Macrolex® Red and Rhodamine 101. As can be seen (ESI Figure S-21), only minor degradation (3%) of PhOHCl-DAOTA was detected even after 1 h of continuous illumination. In the same conditions about 1% of Macrolex® Red and 15% of Rhodamine 101 degraded, confirming excellent photostability of the triangulenium chromophore.

pH Optodes

pH optodes were manufactured via physical entrapment of the indicator dyes into a polyurethane hydrogel D4 (water uptake 50%). Evidently, the spectral properties of the immobilized indicators are very similar to the dissolved ones (Figure **2**). Even at high concentrations (1% wt.) the absorption spectra remain virtually unaltered (Figure **2**a) which indicates absence of dye aggregation.

Deprotonation of the receptor results in a minor bathochromic shift of the absorption spectra and almost complete quenching of fluorescence (Figure **2**b). This response is reversible, showing almost no hysteresis (ESI Figure S-22). Similar to the behaviour in solution, Morph-DAOTA immobilized into D4 hydrogel did not show any pH sensitivity in the pH range from 3 to 12. (ESI Figure S-23).

Despite the positive charge of the triangulenium dyes in the protonated form and zwitterionic character of the deprotonated species, the optodes showed no leaching of the indicators in aqueous media during exposure to various buffers for several hours/overnight (ESI Figure S-24). This confirms the efficiency of the strategy based on a lipophilic anchor group in the indicator molecule.

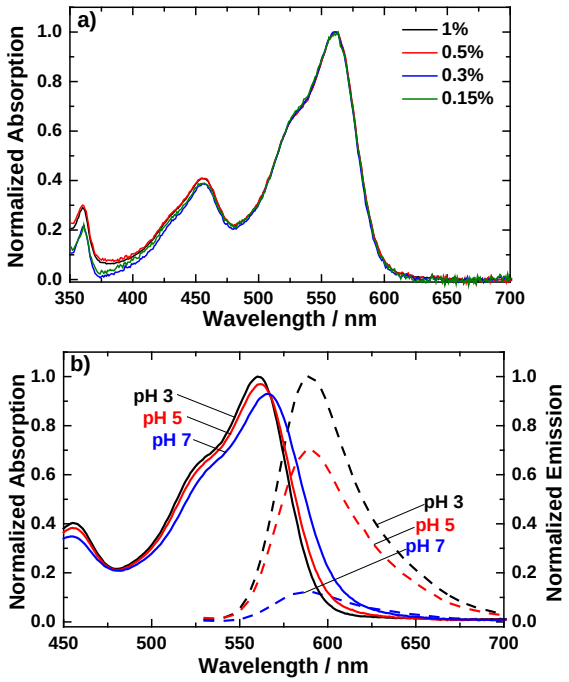

Figure 2: a) Absorption spectra of different concentrations of $PhOHCl_2$-DAOTA in D4. **b)** pH dependency of the absorption and emission (λ_{exc} = 560 nm) spectra of $PhOHCl_2$-DAOTA dye 1% wt. in D4.

pH Dependence of Fluorescence Intensity

Similar to solutions (Figure **1**b), the pH sensors show typical sigmoidal dependency of both fluorescence intensity and decay time. As expected, the sensors based on $PhOHCl_2$-DAOTA and PhOHCl-DAOTA indicators cover different dynamic ranges (Figure **3**a) making them suitable for a variety of potential applications ranging from biotechnology to biology and medicine.

The cross-talk of optical pH sensors to ionic strength resulting from different charges of the protonated and deprotonated forms is well documented in literature. Not surprisingly, this cross-talk was also observed for the sensors based on triangulenium dyes (Figure **3**b). In fact, the apparent pK'_a value of the of $PhOHCl_2$-DAOTA embedded into D4 hydrogel (1% wt. of the dye) increased from

4.71 ± 0.01 to 5.00 ± 0.04 on going from 10 mM NaCl to 290 mM NaCl (overall ionic strength of ~ 20 and 300 mM, respectively).

Subsequently, we investigated the effect of different cations and anions on the pH sensing behaviour of D4-immobilized $PhOHCl_2$-DAOTA, keeping total ionic strength constant. Whereas several common metal cations used in physiologically relevant concentrations did not affect the fluorescence properties of the sensor (ESI Figure S-25), we found a strong influence of the anion nature on the response curve (Figure **3**b). In fact, the apparent pK'_a value increased from 5.00 ± 0.04 for 290 mM NaCl to 5.38 ± 0.04 for 290 mM $NaNO_3$. This shift was even more pronounced in presence of the perchlorate ion (addition of 100 mM $NaClO_4$ to 190 mM NaCl); the material showing the apparent pK'_a value of 5.54 ± 0.09. Importantly, the nature of the anions similarly affects the apparent pK'_a values obtained from the absorption spectra (Figure **3**c). Interestingly, the observed trend correlates well with the position of the anions in the Hofmeister series.[50]

Polyurethane hydrogels are reported to be heterogeneous featuring microphase separation and physical cross-linking typical for polyurethanes[51] which is due to combination of hydrophobic interactions (aggregation of hydrophobic domains in order to minimize the surface area contacting with bulk water)[52] and hydrogen bonding between NH groups and urethane carbonyl oxygen or ether oxygen atoms.[53] Therefore, the above behaviour may be due to formation of stable ion pairs between the dye and the anion and the associated changes in the dye localization in the heterogeneous hydrogel matrix. This can affect both the fluorescence properties and dissociation equilibrium due to different activity of the protons and changes in microsolvation in the not purely aqueous medium. In fact, only marginal difference between the pK_a values obtained in 290 mM NaCl and 290 mM $NaNO_3$ were observed for the dissolved indicator (Figure **1**b). Moreover, whereas in solution the emission intensity of the dye appears not to be affected by the nature of the anion (ESI Figure S-20), the situation is opposite for the hydrogel-immobilized dye (Figure **3**d). Here a strong enhancement of the fluorescence intensity in the row $Cl^- < NO_3^- < ClO_4^-$ was observed. Immobilization of the indicator into the blends of hydrogel D4 and Nafion® 117 membrane (a perfluorinated polymer with charged sulfonate-groups) virtually eliminated the anion interference albeit at the cost of strong dependency of the apparent pK_a of the indicator to ionic strength explained by the highly charged character of the matrix (ESI Figure S-27). Based on above considerations, immobilization of the triangulenium indicators into homogeneous polymeric matrixes (e.g. acrylamides, acrylates etc.) or their covalent attachment to the polymer support (e.g. cross-linked polymeric microparticles, silica-gel beads etc.) should be considered in future as a possible way to minimize the anion influence.

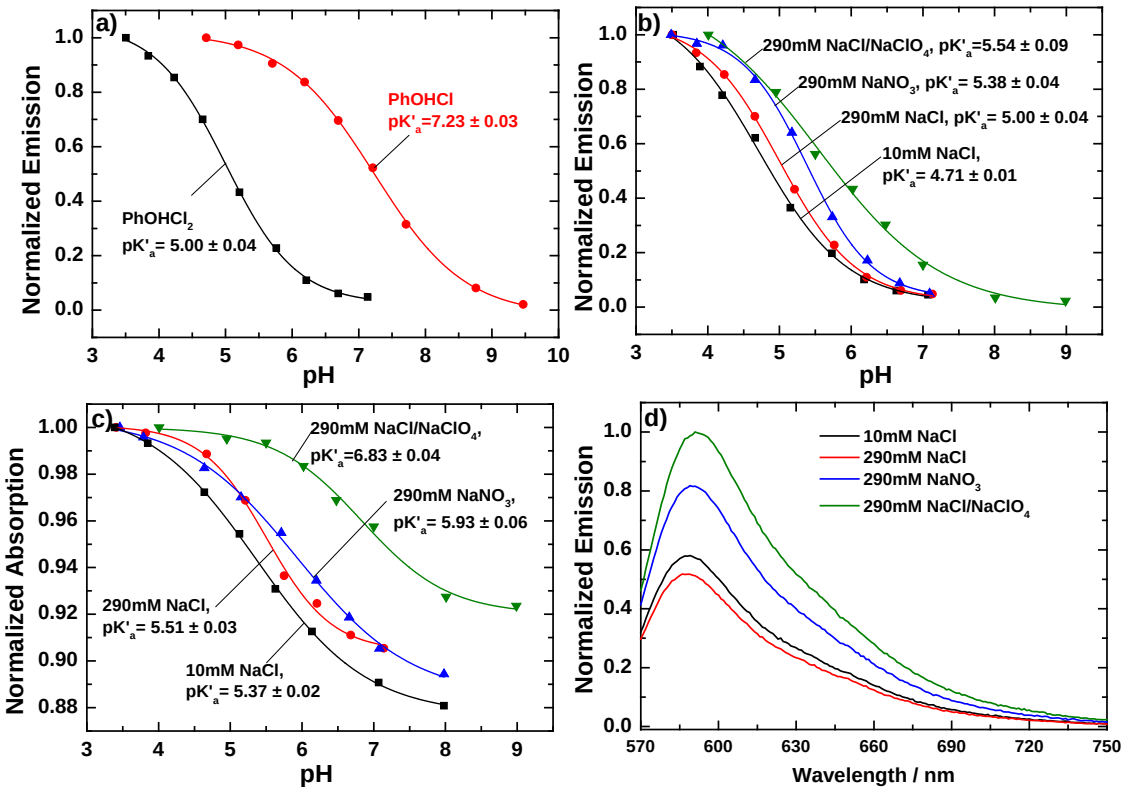

Figure 3: a) Fluorescence response of the $PhOHCl_2$-DAOTA and PhOHCl-DAOTA embedded into hydrogel D4 (1% wt. of the dye, 290 mM NaCl); **b)** and **c)** pH dependency of fluorescence (λ = 590 nm) and absorption (λ = 560 nm), respectively, of $PhOHCl_2$-DAOTA in D4 (1% wt. of the dye) in buffers with different ionic strength and type of anions; **d)** Influence of ionic strength and type of anion on the fluorescence intensity of the same material measured at pH 3; buffer concentrations in all cases 10 mM; (λ_{exc} = 560 nm).

pH Dependence of Fluorescence Decay Time

Fluorescence lifetime measurements in EtOH:buffer solutions revealed that the decay time was independent on pH (17.3 ns, ESI Figure S-28). Such behaviour is not unexpected since only the protonated form of the dye is emissive and "visible" for the decay time measurement. In contrast, a clear pH dependency of the average decay time was observed for the polymer-immobilized dyes (Figure **4**). More detailed investigation revealed strong dependency of the calibration plots on the concentration of the immobilized dye (Figure **4**).

This unexpected lifetime sensitivity is attributed to the homo-FRET process. In fact, the overlap between absorption and emission spectra is clearly visible (Figure **2**). Moreover, despite rather modest bathochromic shift of the absorption spectrum, the overlap increases significantly upon deprotonation of the dye. The FRET efficiency and the observed lifetime change is the highest for 1% dye doping (~2-fold lifetime change from pH 3 to pH 8). On the contrary, it is the least pronounced (only 15% decrease in the same pH range) for the lowest concentration of the dye in the polymer

(0.15% wt.). Nevertheless, even the lowest concentration of the dye in the optode is much higher than for the solutions (~2.5 mM for the swollen hydrogel and 10 µM for the solution) where no lifetime change was recorded. Clearly, because of the self-referenced character of the decay time, the new materials are very promising for a lifetime-based micro- and macroscopic imaging using a FLIM technique. Imaging of pH with planar optodes gains importance in marine biology[54,55], soil and plant research[4,5], medicine[7] and other areas and is currently performed either in ratiometric mode or using a so called dual lifetime referencing technique. These methods typically require addition of other luminescent reference emitters which makes the system more complex and does not eliminate some interferences (e.g. from light scattering or background fluorescence). The advantage of the new optode for lifetime imaging of pH is strong modulation of the decay time which however remains sufficiently long to discard the autofluorescence from the sample. Moreover, the decay only slightly deviates from the mono-exponential behaviour (ESI Figure S-29) which can also be useful for background elimination and simplified data processing.

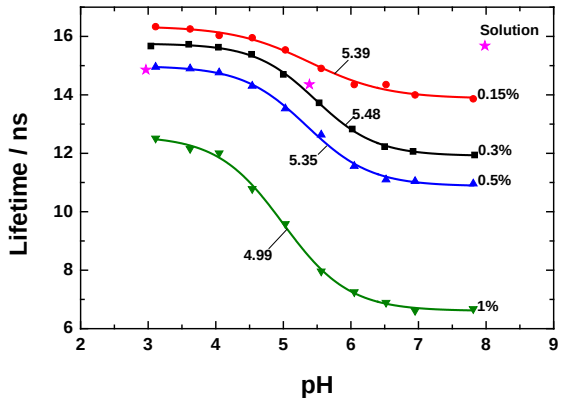

Figure 4: Response of the fluorescence lifetimes to pH for different concentrations of $PhOHCl_2$-DAOTA in D4 (% wt.) and of 10 µM dye solution (MeOH:buffer 30:70) at 25 °C, 10 mM buffer and 140 mM NaCl; the inflection points of the curves are marked in the graph.

FD-FLIM imaging with the planar optodes

In order to demonstrate the practical applicability of the sensors we interrogated them with a new frequency-domain lifetime imaging camera, pco.flim.[44,45] The pH dependencies of the fluorescence decay time obtained in the imaging experiments (Figure **5a**) and TCSPC (Figure **4**) are similar. The planar optode placed inside the chamber of a microfluidic chip (Figure **5b**) proved to be excellently suitable for monitoring of pH gradients (Figure **5c** and **5d**). This can be useful, for instance, for monitoring enzymatic reactions[56] and for isoelectric focusing.[9,10] The experiment also shows that the planar optode in combination with the FD-FLIM camera can also be used on macroscale for other experiments, for example monitoring pH in biofilms[6] or during wound healing.[7,8]

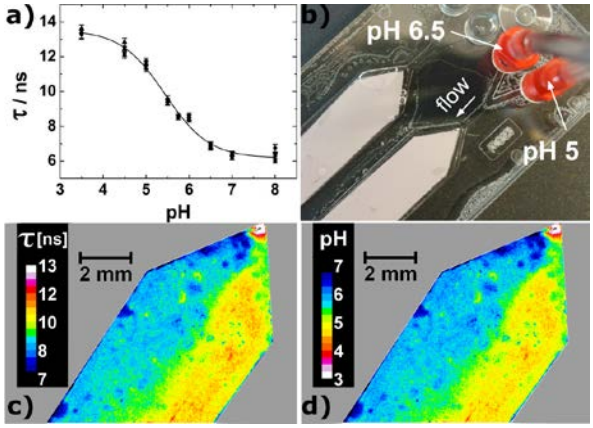

Figure 5: FLIM imaging of pH with the planar optode based on $PhOHCl_2$-DAOTA in D4 (1 % wt). (**a**): pH dependency of the fluorescence lifetime obtained in the microscopic imaging experiment (read-out area ~0.9x0.9 mm). The foil has been measured at ≥ 3 different spots for each pH value. (**b**): photographic image of the microfluidic chip with integrated sensor foil. (**c**) and (**d**): false color images of decay time and pH distribution, respectively, for the microfluidic chip simultaneously flushed with buffers of pH 6.5 and 5.0 (speed 21 µL min^{-1}).

pH nanosensors

Several types of nanoparticles with immobilized indicators were prepared in order to explore the self-referenced lifetime measuring capabilities. In order to ensure high efficiency of homo-FRET, comparably high concentration of the dye was used (0.75% wt.). Nanoparticles prepared upon immobilization of $PhOHCl_2$-DAOTA into anionic PMMA-MA showed aggregation in buffer solutions, which might be due to destabilization of the particle by the cationic dye. The cationic RL-100 nanoparticles (Z-potential of +41 mV), on the contrary, were stable in water and in buffers. Their size (16 nm, PDI=0.410) was significantly below the size of the RL-100 particles doped with a hydrophobic oxygen indicator (30-40 nm).[57,58] The dyes showed no leaching from the nanoparticles in aqueous buffer solution evidenced by formation of colored precipitate and uncoloured solution upon coagulation of the beads at high concentration (~3 mg/mL) and high ionic strength (300 mM). For both dyes in RL-100 nanoparticles, pH calibrations in fluorescence intensity and decay time mode yielded sigmoidal calibration plots (ESI, Figure S-31).

$PhOHCl_2$-DAOTA was also immobilized in poly(styrene-sulfonic acid) (PSSA) which forms very small (6 nm) and highly negatively-charged (Z-potential of -49 mV) nanogel. The fluorescence intensity decreased by about 80% on going from pH 4.5 to 7.5, showing the characteristic sigmoidal response with an apparent pK'_a of 5.98. Change in fluorescence decay time, however, was not observed. This indicates that the PSSA dispersion cannot provide the spatial proximity necessary for efficient homo-FRET.

As expected, the inflection point of decay time measurements for $PhOHCl_2$-DAOTA embedded in the positively charged RL-100 nanoparticles was about one pH unit lower than in the

uncharged hydrogel D4 (4.02 and 5.00, respectively). On the contrary, the pK_a' value for the dye in negatively charged PSSA (5.98) was about one pH unit higher than in D4.

Due to the possibility of the self-referenced read-out, the Rl-100 based nanosensors were expected to be highly promising for intracellular pH imaging. Although they showed no evident toxicity after internalization by the human colon cancer HCT116 cells (ESI, Fig. S-32), the staining was very fast (1 h or less) and highly similar to the free dye, which may indicate leaching of the dye from the nanoparticles inside the cells, due to their small size (ESI, Fig. S-33, S-34). For comparison, the nanoparticles prepared from the same polymer typically require three hours and more for cell internalization.[58,59] The assumption of leaching was also supported by the FLIM measurements in cells, when no reliable pH response and loss of mitochondrial-like localization after dissipation of mitochondrial pH gradient were observed (ESI, Fig. S-35, S-36). Therefore, for intracellular pH FLIM sensing, it appears to be essential to completely eliminate 'in-cell' leaching of the dye out of the nanosensors, which can be possible by using longer (or/and branched) anchor groups or via covalent grafting of the indicators into the polymer.

CONCLUSIONS

In this work, we presented synthesis and characterization of new fluorescent pH indicators based on diazaoxatriangulenium dyes. The dyes were rationally designed to bear both a pH-sensing functionality and a hydrophobic anchor group for non-covalent immobilization into hydrogel matrices and nanoparticles. The dyes feature absorption and emission in the green-orange part of the spectrum and possess excellent photostability. Importantly, the pH indicators retain extremely long fluorescence decay times enabling efficient elimination of autofluorescence in time-resolved measurements.

Chlorinated phenols proved to be excellent receptors, which enable pH modulation via photoinduced electron transfer. The dyes decorated with mono- and di-chlorinated moieties possess largely different pK'_a values and therefore enable high versatility of potential applications. Unexpectedly, we have found strong pH dependency of the fluorescence decay time for the indicators immobilized into a polyurethane hydrogel and polymeric nanoparticles. Being concentration-dependent and not observed for the dissolved indicators this behaviour is attributed to homo-FRET. Self-referenced character of the lifetime measurement makes the new materials particularly attractive for pH sensing and imaging. Whereas pH measurement in cells with help of nanosensors proved to be impossible due to dye leaching in the intracellular environment, the planar optodes were shown to be promising for imaging of pH distribution with help of a FD-FLIM camera. This paves the way to a variety of applications eliminating the need for the reference luminophore which so far has to be added into the sensing material for reliable measurement. Covalent immobilization of the dyes into the polymers represent the next logical step in order to eliminate leaching of the indicators out of the

nanoparticles and possibly reduce the cross-sensitivity of the sensor response to the nature of anion used.

ACKNOWLEDGMENTS

This work was partly supported by the Science Foundation Ireland (SFI) grant 13/SIRG/2144 (RID). The authors thank Prof. T. Mayr (TU Graz) for providing the microfluidic chips.

SUPPORTING INFORMATION

Additional Experimental Data. Analytical data for structure analysis (^{1}H, COSY, APT and HSQC NMR, Maldi-TOF MS) Figures S1-S19. Details on characterization of optodes (leaching, reversibility, hysteresis, calibration, interferences and cell staining / viability / FLIM studies, Figures S20-S36).

REFERENCES

(1) McDonagh, C.; Burke, C. S.; MacCraith, B. D. Optical Chemical Sensors. *Chem. Rev.* **2008**, *108* (2), 400–422. https://doi.org/10.1021/cr068102g.

(2) Stahl, H.; Glud, A.; Schröder, C. R.; Klimant, I.; Tengberg, A.; Glud, R. N. Time-Resolved PH Imaging in Marine Sediments with a Luminescent Planar Optode: PH Imaging in Marine Sediments. *Limnol. Oceanogr. Methods* **2006**, *4* (10), 336–345. https://doi.org/10.4319/lom.2006.4.336.

(3) Larsen, M.; Borisov, S. M.; Grunwald, B.; Klimant, I.; Glud, R. N. A Simple and Inexpensive High Resolution Color Ratiometric Planar Optode Imaging Approach: Application to Oxygen and PH Sensing.: A Simple RGB Based Planar Optode Imaging Approach. *Limnol. Oceanogr. Methods* **2011**, *9* (9), 348–360. https://doi.org/10.4319/lom.2011.9.348.

(4) Hoefer, C.; Santner, J.; Borisov, S. M.; Wenzel, W. W.; Puschenreiter, M. Integrating Chemical Imaging of Cationic Trace Metal Solutes and PH into a Single Hydrogel Layer. *Anal. Chim. Acta* **2017**, *950*, 88–97. https://doi.org/10.1016/j.aca.2016.11.004.

(5) Koop-Jakobsen, K.; Mueller, P.; Meier, R. J.; Liebsch, G.; Jensen, K. Plant-Sediment Interactions in Salt Marshes – An Optode Imaging Study of O2, PH, and CO2 Gradients in the Rhizosphere. *Front. Plant Sci.* **2018**, *9*. https://doi.org/10.3389/fpls.2018.00541.

(6) Moßhammer, M.; Strobl, M.; Kühl, M.; Klimant, I.; Borisov, S. M.; Koren, K. Design and Application of an Optical Sensor for Simultaneous Imaging of PH and Dissolved O_2 with Low Cross-Talk. *ACS Sens.* **2016**, *1* (6), 681–687. https://doi.org/10.1021/acssensors.6b00071.

(7) Schreml, S.; Meier, R. J.; Wolfbeis, O. S.; Landthaler, M.; Szeimies, R.-M.; Babilas, P. 2D Luminescence Imaging of PH in Vivo. *Proc. Natl. Acad. Sci.* **2011**, *108* (6), 2432–2437. https://doi.org/10.1073/pnas.1006945108.

(8) Meier, R. J.; Schreml, S.; Wang, X.; Landthaler, M.; Babilas, P.; Wolfbeis, O. S. Simultaneous Photographing of Oxygen and PH In Vivo Using Sensor Films. *Angew. Chem.* **2011**, *123* (46), 11085–11088. https://doi.org/10.1002/ange.201104530.

(9) Jezierski, S.; Belder, D.; Nagl, S. Microfluidic Free-Flow Electrophoresis Chips with an Integrated Fluorescent Sensor Layer for Real Time PH Imaging in Isoelectric Focusing. *Chem Commun* **2013**, *49* (9), 904–906. https://doi.org/10.1039/C2CC38093E.

(10) Poehler, E.; Herzog, C.; Lotter, C.; Pfeiffer, S. A.; Aigner, D.; Mayr, T.; Nagl, S. Label-Free Microfluidic Free-Flow Isoelectric Focusing, PH Gradient Sensing and near Real-Time Isoelectric Point Determination of Biomolecules and Blood Plasma Fractions. *The Analyst* **2015**, *140* (22), 7496–7502. https://doi.org/10.1039/C5AN01345C.

(11) Han, J.; Burgess, K. Fluorescent Indicators for Intracellular PH. *Chem. Rev.* **2010**, *110* (5), 2709–2728. https://doi.org/10.1021/cr900249z.

(12) Offenbacher, H.; Wolfbeis, O. S.; Fürlinger, E. Fluorescence Optical Sensors for Continuous Determination of Near-Neutral PH Values. *Sens. Actuators* **1986**, *9* (1), 73–84. https://doi.org/10.1016/0250-6874(86)80008-7.

(13) Whitaker, J. E.; Haugland, R. P.; Prendergast, F. G. Spectral and Photophysical Studies of Benzo[c]Xanthene Dyes: Dual Emission PH Sensors. *Anal. Biochem.* **1991**, *194* (2), 330–344. https://doi.org/10.1016/0003-2697(91)90237-N.

(14) Wolfbeis, O. S.; Fürlinger, E.; Kroneis, H.; Marsoner, H. Fluorimetric Analysis: 1. Untersuchung von Fluorescenzindicatoren Zur Messung von PH-Werten Im Neutralbereich. *Fresenius Z. Für Anal. Chem.* **1983**, *314* (2), 119–124. https://doi.org/10.1007/BF00482235.

(15) Zhujun, Z.; Seitz, W. R. A Fluorescence Sensor for Quantifying PH in the Range from 6.5 to 8.5. *Anal. Chim. Acta* **1984**, *160*, 47–55. https://doi.org/10.1016/S0003-2670(00)84507-9.

(16) Niu, C.-G.; Zeng, G.-M.; Chen, L.-X.; Shen, G.-L.; Yu, R.-Q. Proton "'off-on'" Behaviour of Methylpiperazinyl Derivative of Naphthalimide: A PH Sensor Based on Fluorescence Enhancement. *The Analyst* **2004**, *129* (1), 20–24. https://doi.org/10.1039/B309594K.
(17) Li, Z.-Z.; Niu, C.-G.; Zeng, G.-M.; Liu, Y.-G.; Gao, P.-F.; Huang, G.-H.; Mao, Y.-A. A Novel Fluorescence Ratiometric PH Sensor Based on Covalently Immobilized Piperazinyl-1,8-Napthalimide and Benzothioxanthene. *Sens. Actuators B Chem.* **2006**, *114* (1), 308–315. https://doi.org/10.1016/j.snb.2005.05.018.
(18) Gotor, R.; Ashokkumar, P.; Hecht, M.; Keil, K.; Rurack, K. Optical PH Sensor Covering the Range from PH 0–14 Compatible with Mobile-Device Readout and Based on a Set of Rationally Designed Indicator Dyes. *Anal. Chem.* **2017**, *89*, 8437–8444. https://doi.org/10.1021/acs.analchem.7b01903.
(19) Strobl, M.; Walcher, A.; Mayr, T.; Klimant, I.; Borisov, S. M. Trace Ammonia Sensors Based on Fluorescent Near-Infrared-Emitting Aza-BODIPY Dyes. *Anal. Chem.* **2017**, *89* (5), 2859–2865. https://doi.org/10.1021/acs.analchem.6b04045.
(20) Tahirbegi, I. B.; Ehgartner, J.; Sulzer, P.; Zieger, S.; Kasjanow, A.; Paradiso, M.; Strobl, M.; Bouwes, D.; Mayr, T. Fast Pesticide Detection inside Microfluidic Device with Integrated Optical PH, Oxygen Sensors and Algal Fluorescence. *Biosens. Bioelectron.* **2017**, *88*, 188–195. https://doi.org/10.1016/j.bios.2016.08.014.
(21) Szmacinski, H.; Lakowicz, J. R. Optical Measurements of PH Using Fluorescence Lifetimes and Phase-Modulation Fluorometry. *Anal. Chem.* **1993**, *65* (13), 1668–1674. https://doi.org/10.1021/ac00061a007.
(22) Staudinger, C.; Borisov, S. M. Long-Wavelength Analyte-Sensitive Luminescent Probes and Optical (Bio)Sensors. *Methods Appl. Fluoresc.* **2015**, *3* (4), 042005. https://doi.org/10.1088/2050-6120/3/4/042005.
(23) Clarke, Y.; Xu, W.; Demas, J. N.; DeGraff, B. A. Lifetime-Based PH Sensor System Based on a Polymer-Supported Ruthenium(II) Complex. *Anal. Chem.* **2000**, *72* (15), 3468–3475. https://doi.org/10.1021/ac000111g.
(24) Gonçalves, H. M. R.; Maule, C. D.; Jorge, P. A. S.; Esteves da Silva, J. C. G. Fiber Optic Lifetime PH Sensing Based on Ruthenium(II) Complexes with Dicarboxybipyridine. *Anal. Chim. Acta* **2008**, *626* (1), 62–70. https://doi.org/10.1016/j.aca.2008.07.044.
(25) Malins, C.; Glever, H. .; Keyes, T. .; Vos, J. .; Dressick, W. .; MacCraith, B. . Sol–Gel Immobilised Ruthenium(II) Polypyridyl Complexes as Chemical Transducers for Optical PH Sensing. *Sens. Actuators B Chem.* **2000**, *67* (1–2), 89–95. https://doi.org/10.1016/S0925-4005(00)00411-1.
(26) Blair, S.; Lowe, M. P.; Mathieu, C. E.; Parker, D.; Senanayake, P. K.; Kataky, R. Narrow-Range Optical PH Sensors Based on Luminescent Europium and Terbium Complexes Immobilized in a Sol Gel Glass. *Inorg. Chem.* **2001**, *40* (23), 5860–5867. https://doi.org/10.1021/ic010371w.
(27) Ryder, A. G.; Power, S.; Glynn, T. J. Evaluation of Acridine in Nafion as a Fluorescence-Lifetime-Based PH Sensor. *Appl. Spectrosc.* **2003**, *57* (1), 73–79.
(28) Lin, H.-J.; Szmacinski, H.; Lakowicz, J. R. Lifetime-Based PH Sensors: Indicators for Acidic Environments. *Anal. Biochem.* **1999**, *269* (1), 162–167. https://doi.org/10.1006/abio.1999.4011.
(29) Aigner, D.; Dmitriev, R. I.; Borisov, S. M.; Papkovsky, D. B.; Klimant, I. PH-Sensitive Perylene Bisimide Probes for Live Cell Fluorescence Lifetime Imaging. *J Mater Chem B* **2014**, *2* (39), 6792–6801. https://doi.org/10.1039/C4TB01006J.
(30) Orte, A.; Alvarez-Pez, J. M.; Ruedas-Rama, M. J. Fluorescence Lifetime Imaging Microscopy for the Detection of Intracellular PH with Quantum Dot Nanosensors. *ACS Nano* **2013**, *7* (7), 6387–6395. https://doi.org/10.1021/nn402581q.
(31) Tang, R.; Lee, H.; Achilefu, S. Induction of PH Sensitivity on the Fluorescence Lifetime of Quantum Dots by NIR Fluorescent Dyes. *J. Am. Chem. Soc.* **2012**, *134* (10), 4545–4548. https://doi.org/10.1021/ja300276s.
(32) Chen, C.; Zhang, P.; Zhang, L.; Gao, D.; Gao, G.; Yang, Y.; Li, W.; Gong, P.; Cai, L. Long-Decay near-Infrared-Emitting Doped Quantum Dots for Lifetime-Based in Vivo PH

Imaging. *Chem. Commun.* **2015**, *51* (56), 11162–11165. https://doi.org/10.1039/C5CC03046C.
(33) Rich, R. M.; Stankowska, D. L.; Maliwal, B. P.; Sørensen, T. J.; Laursen, B. W.; Krishnamoorthy, R. R.; Gryczynski, Z.; Borejdo, J.; Gryczynski, I.; Fudala, R. Elimination of Autofluorescence Background from Fluorescence Tissue Images by Use of Time-Gated Detection and the AzaDiOxaTriAngulenium (ADOTA) Fluorophore. *Anal. Bioanal. Chem.* **2013**, *405* (6), 2065–2075. https://doi.org/10.1007/s00216-012-6623-1.
(34) Draxler, S.; Lippitsch, M. E. PH Sensors Using Fluorescence Decay Time. *Sens. Actuators B Chem.* **1995**, *29* (1–3), 199–203. https://doi.org/10.1016/0925-4005(95)01683-X.
(35) Badri P., M.; Rafal, F.; Sangram, R.; Rutika, K.; Thomas J., S.; Bo W., L.; Zygmunt, G.; Ignacy, G. Long-Lived Bright Red Emitting Azaoxa-Triangulenium Fluorophores. *PLoS ONE* **2013**, *8* (5). https://doi.org/10.1371/journal.pone.0063043.
(36) Westerlund, F.; Hildebrandt, C. B.; Sørensen, T. J.; Laursen, B. W. Trihydroxytrioxatriangulene-An Extended Fluorescein and a Ratiometric PH Sensor. *Chem. - Eur. J.* **2010**, *16* (10), 2992–2996. https://doi.org/10.1002/chem.200902965.
(37) Frankær, C. G.; Hussain, K. J.; Rosenberg, M.; Jensen, A.; Laursen, B. W.; Sørensen, T. J. Biocompatible Microporous Organically Modified Silicate Material with Rapid Internal Diffusion of Protons. *ACS Sens.* **2018**, *3* (3), 692–699. https://doi.org/10.1021/acssensors.8b00024.
(38) Laursen, B. W.; Sorensen, T. J.; (Vorname). Synthesis of Super Stable Triangulenium Dye. *J. Org. Chem.* **2009**, *74* (8), 3183–3185. https://doi.org/10.1021/jo9002486.
(39) Laursen, B. W.; Krebs, F. C.; Nielsen, M. F.; Bechgaard, K.; Christensen, J. B.; Harrit, N. 2,6,10-Tris(Dialkylamino)Trioxatriangulenium Ions. Synthesis, Structure, and Properties of Exceptionally Stable Carbenium Ions. *J. Am. Chem. Soc.* **1998**, *120* (47), 12255–12263. https://doi.org/10.1021/ja982550r.
(40) Laursen, B. W.; Krebs, F. C. Synthesis, Structure, and Properties of Azatriangulenium Salts. *Chem. - Eur. J.* **2001**, *7* (8), 1773–1783. https://doi.org/10.1002/1521-3765(20010417)7:8<1773::AID-CHEM17730>3.0.CO;2-F.
(41) Wittig, G.; Pockels, U. Über Den Austausch von Aromatisch Gebundenem Brom Gegen Lithium Mittels Phenyl-Lithiums. *Berichte Dtsch. Chem. Ges.* **1939**, *72*, 89–92. https://doi.org/10.1002/cber.19390720120.
(42) Martin, J. C.; Smith, R. G. Factors Influencing the Basicities of Triarylcarbinols. The Synthesis of Sesquixanthydrol. *J. Am. Chem. Soc.* **1964**, *86* (11), 2252–2256. https://doi.org/10.1021/ja01065a030.
(43) Seybold, G. New Perylene and Violanthrone Dyestuffs for Fluorescent Collectors. *Dyes Pigments* **1989**, *11* (4), 303–317. https://doi.org/10.1016/0143-7208(89)85048-X.
(44) Chen, H.; Holst, G.; Gratton, E. Modulated CMOS Camera for Fluorescence Lifetime Microscopy: Modulated CMOS Camera for Fluorescence Lifetime Microscopy. *Microsc. Res. Tech.* **2015**, *78* (12), 1075–1081. https://doi.org/10.1002/jemt.22587.
(45) Franke, R.; Holst, G. A. Frequency-Domain Fluorescence Lifetime Imaging System (Pco.Flim) Based on a in-Pixel Dual Tap Control CMOS Image Sensor. *SPIE Proceedings*; **2015**; Vol. 9328, pp 93281K-9328–19.
(46) Aigner, D.; Freunberger, S. A.; Wilkening, M.; Saf, R.; Borisov, S. M.; Klimant, I. Enhancing Photoinduced Electron Transfer Efficiency of Fluorescent PH-Probes with Halogenated Phenols. *Anal. Chem.* **2014**, *86* (18), 9293–9300. https://doi.org/10.1021/ac502513g.
(47) Bogh, S. A.; Simmermacher, M.; Westberg, M.; Bregnhøj, M.; Rosenberg, M.; De Vico, L.; Veiga, M.; Laursen, B. W.; Ogilby, P. R.; Sauer, S. P. A.; et al. Azadioxatriangulenium and Diazaoxatriangulenium: Quantum Yields and Fundamental Photophysical Properties. *ACS Omega* **2017**, *2* (1), 193–203. https://doi.org/10.1021/acsomega.6b00211.
(48) Huber, C.; Klimant, I.; Krause, C.; Wolfbeis, O. S. Dual Lifetime Referencing as Applied to a Chloride Optical Sensor. *Anal. Chem.* **2001**, *73* (9), 2097–2103. https://doi.org/10.1021/ac9914364.

(49) Masih, D.; Aly, S. M.; Alarousu, E.; Mohammed, O. F. Photoinduced Triplet-State Electron Transfer of Platinum Porphyrin: A One-Step Direct Method for Sensing Iodide with an Unprecedented Detection Limit. *J. Mater. Chem. A* **2015**, *3* (13), 6733–6738. https://doi.org/10.1039/C4TA07033J.
(50) Baldwin, R. L. How Hofmeister Ion Interactions Affect Protein Stability. *Biophys. J.* **1996**, *71* (4), 2056–2063. https://doi.org/10.1016/S0006-3495(96)79404-3.
(51) Fernández-d´Arlas, B.; Rueda, L.; Fernández, R.; Khan, U.; Coleman, J. N.; Mondragon, I.; Eceiza, A. Inverting Polyurethanes Synthesis: Effects on Nano/Micro-Structure and Mechanical Properties. *Soft Mater.* **2010**, *9* (1), 79–93. https://doi.org/10.1080/1539445X.2010.525173.
(52) Hoare, T. R.; Kohane, D. S. Hydrogels in Drug Delivery: Progress and Challenges. *Polymer* **2008**, *49* (8), 1993–2007. https://doi.org/10.1016/j.polymer.2008.01.027.
(53) Furukawa, M.; Kojio, K.; Kugumiya, S.; Uchiba, Y.; Mitsui, Y. Microphase Separation of Bulk and Ultrathin Films of Polyurethane Elastomers. *Macromol. Symp.* **2008**, *267* (1), 9–15. https://doi.org/10.1002/masy.200850702.
(54) Kühl, M.; Polerecky, L. Functional and Structural Imaging of Phototrophic Microbial Communities and Symbioses. *Aquat. Microb. Ecol.* **2008**, *53*, 99–118. https://doi.org/10.3354/ame01224.
(55) Han, C.; Yao, L.; Xu, D.; Xie, X.; Zhang, C. High-Resolution Imaging of PH in Alkaline Sediments and Water Based on a New Rapid Response Fluorescent Planar Optode. *Sci. Rep.* **2016**, *6* (1). https://doi.org/10.1038/srep26417.
(56) Gruber, P.; Marques, M. P. C.; Sulzer, P.; Wohlgemuth, R.; Mayr, T.; Baganz, F.; Szita, N. Real-Time PH Monitoring of Industrially Relevant Enzymatic Reactions in a Microfluidic Side-Entry Reactor (MSER) Shows Potential for PH Control. *Biotechnol. J.* **2017**, *12* (6), 1600475. https://doi.org/10.1002/biot.201600475.
(57) Fercher, A.; Borisov, S. M.; Zhdanov, A. V.; Klimant, I.; Papkovsky, D. B. Intracellular O2 Sensing Probe Based on Cell-Penetrating Phosphorescent Nanoparticles. *ACS Nano* **2011**, *5* (7), 5499–5508. https://doi.org/10.1021/nn200807g.
(58) Müller, B. J.; Zhdanov, A. V.; Borisov, S. M.; Foley, T.; Okkelman, I. A.; Tsytsarev, V.; Tang, Q.; Erzurumlu, R. S.; Chen, Y.; Zhang, H.; et al. Nanoparticle-Based Fluoroionophore for Analysis of Potassium Ion Dynamics in 3D Tissue Models and In Vivo. *Adv. Funct. Mater.* **2018**, *28* (9), 1704598. https://doi.org/10.1002/adfm.201704598.
(59) Dmitriev, R. I.; Borisov, S. M.; Düssmann, H.; Sun, S.; Müller, B. J.; Prehn, J.; Baklaushev, V. P.; Klimant, I.; Papkovsky, D. B. Versatile Conjugated Polymer Nanoparticles for High-Resolution O $_2$ Imaging in Cells and 3D Tissue Models. *ACS Nano* **2015**, *9* (5), 5275–5288. https://doi.org/10.1021/acsnano.5b00771.

For TOC only

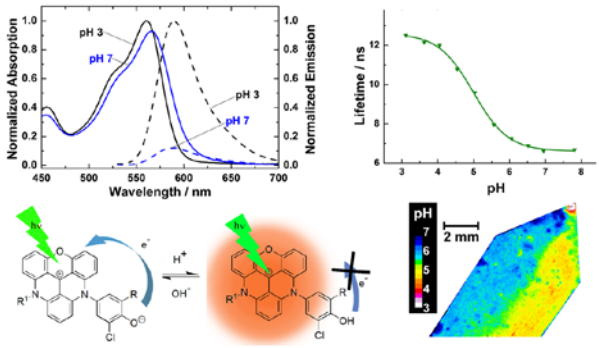
Normalized Absorption
Normalized Emission
Wavelength / nm
pH 3
pH 7
Lifetime / ns
pH
2 mm
hν
e⁻
H⁺
OH⁻